

Steady Spins and Spinup Dynamics of Axisymmetric Dual-Spin Satellites with Dampers *

Ralph A. Sandfry[†] and Christopher D. Hall[‡]

We investigate the possible equilibria of dual-spin satellites by studying a torque-free gyrostator with an attached spring-mass damper. Using numerical continuation we present possible equilibria for axisymmetric dual-spin satellites and also show how slight inertia asymmetries affect equilibria. Even small asymmetries can significantly change the location of off-nominal steady spins. Also, the existence of certain equilibria is related to a simple damper tuning condition. Finally, the bifurcation diagrams for varying rotor momentum provide a useful perspective of rotor spinup dynamics.

* This paper is declared a work of the U.S. Government and is not subject to copyright protection in the United States

[†]Formerly PhD Candidate, Aerospace and Ocean Engineering, Virginia Polytechnic Institute and State University, Blacksburg, Virginia. Currently, Director of Operations, Detachment 4, Air Force Operational Test and Evaluation Center, Peterson Air Force Base, Colorado 80914. Member AIAA.

[‡]Professor, Aerospace and Ocean Engineering, Virginia Polytechnic Institute and State University, Blacksburg, Virginia 24061. Associate Fellow, AIAA.

Nomenclature

$\hat{\mathbf{a}}$	= rotor spin-axis, rad/s
\mathcal{B}	= rigid body
$\hat{\mathbf{b}}_i$	= body frame axes, $i = 1, 2, 3$
\mathbf{b}	= rest position of damper mass, m
c	= damping coefficient, kg/s
\mathbf{f}	= external force, N
\mathbf{g}	= external torque, N·m
g_a	= rotor torque, N·m
\mathbf{h}	= system angular momentum vector, kg·m ² /s
h_a	= angular momentum of \mathcal{R} about $\hat{\mathbf{a}}$, absolute; $h_a = I_s \hat{\mathbf{a}}^T \boldsymbol{\omega} + h_s$, kg·m ² /s
h_s	= angular momentum of \mathcal{R} about $\hat{\mathbf{a}}$, relative to platform; $h_s = I_s \omega_s$, kg·m ² /s
I	= system inertia matrix when $x = 0$; $I = \text{diag}(I_1, I_2, I_3)$, kg·m ²
I'_1	= $I_1 - I_s$, kg·m ²
I_s	= moment of inertia of \mathcal{R} about $\hat{\mathbf{a}}$, kg·m ²
J	= system inertia matrix, kg·m ²
K	= inertia-like matrix, kg·m ²
k	= spring stiffness, kg/s ²
k_d	= tuned-damper spring stiffness, kg/s ²
\mathbf{m}	= angular momentum-like vector, kg·m ² /s
m	= system mass, kg
m_d	= damper mass, kg

- $\hat{\mathbf{n}}$ = direction of positive damper displacement
- \mathcal{O} = origin of body frame
- \mathcal{P} = damper mass particle
- \mathbf{p} = system linear momentum, kg·m/s
- p_n = linear momentum of \mathcal{P} in $\hat{\mathbf{n}}$ direction, kg·m/s
- \mathcal{R} = rigid axisymmetric rotor
- \mathbf{v}_o = velocity of \mathcal{O} , m/s
- x = damper displacement in $\hat{\mathbf{n}}$ direction, relative to \mathcal{R} , m
- y = damper velocity in $\hat{\mathbf{n}}$ direction, relative to \mathcal{R} , m/s
- ε = m_d/m
- ε' = $1 - \varepsilon$
- λ = dimensionless $h_a - 1$
- $\boldsymbol{\omega}$ = angular velocity of body frame, $\hat{\mathbf{b}}_i$, rad/s
- ω_b = precession frequency, rad/s
- ω_n = natural frequency, rad/s
- ω_s = angular speed of \mathcal{R} relative to \mathcal{B} , rad/s
- $\mathbf{1}$ = identity matrix

Superscript

- * = dimensional quantities

Introduction

For many years satellite designers have successfully used the dual-spin concept for communications satellites, first demonstrated with TACSAT 1.¹ Dual-spin satellites are often modeled as prolate gyrostats with a relatively large rotor aligned with the nominal-spin axis.²⁻⁴ The nominal, steady-spin axis is usually aligned with the spin axis of the large, axisymmetric rotor. Much of the work to date on the gyrostat model has focused on the stability of the nominal spin. Stability in the presence of energy dissipation has been analyzed using energy sink methods^{5,6} and by including the damping mechanism in the gyrostat model^{3,7} However, many equilibria are possible for this system other than the nominal spin. Operational problems and environmental effects always pose the risk of perturbing a satellite, perhaps severely, from its intended attitude. When perturbed, a torque-free gyrostat with damping should eventually reach a stable, although possibly different, equilibrium state. An understanding of the possible equilibrium states is an important step to addressing these operational issues.

This paper investigates the system equilibria for a torque-free gyrostat with typical inertial properties, damper location, and damping coefficient values for a dual-spin satellite, obtained from the literature. The damper spring stiffness is determined by matching the natural frequency of the spring-mass-damper to the satellite precession frequency about the nominal-spin axis. Numerical continuation is used to determine equilibria for varying rotor momentum.⁸ These equilibria are presented on the momentum sphere and as state-parameter bifurcation diagrams. As there are no external torques included, this paper focuses on the rotational motion and equilibria of the gyrostat with realistic parameters. Analysis of this simplified model is a practical

first step prior to considering orbital equilibria with the gravity gradient torque.

An important element of dual-spin satellite dynamics is the dual-spin turn.⁹ Starting with a prolate dual-spin satellite spinning about its major axis, this procedure is used to acquire a stable nominal spin configuration by applying a rotor torque. The reaction torque on the body provides the reorientation from a major to minor axis spin. The path of the spin-axis during the dual-spin turn may not be a simple Euler rotation. This paper demonstrates how, for sufficiently small rotor torques, the spin-axis approximately follows equilibria for increasing rotor momentum.

Equations of Motion

The dual-spin satellite model we study is shown in Fig. 1, consisting of a rigid body, \mathcal{B} , containing a rigid axisymmetric rotor, \mathcal{R} , and a mass particle \mathcal{P} , which is constrained to move along a line $\hat{\mathbf{n}}$ fixed in \mathcal{B} . The axes $\hat{\mathbf{b}}_i$ are system principal axes when \mathcal{P} is in its rest position ($x = 0$). The vector $\hat{\mathbf{n}}$ is parallel to $\hat{\mathbf{b}}_1$, which is the nominal-spin axis for the spacecraft. The particle is connected to a linear spring and has linear damping. The system mass, m , includes the masses of \mathcal{B} , \mathcal{R} , and \mathcal{P} . The spring and damper components are assumed massless other than \mathcal{P} to simplify modeling changes to the moments of inertia. The rotor spin-axis, $\hat{\mathbf{a}}$, is parallel to the $\hat{\mathbf{b}}_1$ axis. All vectors and tensors are expressed with respect to the body frame. This configuration is a reasonable model for a dual-spin spacecraft with a “ball-in-tube” type precession damper. It also can model any spacecraft with a single momentum wheel and a similar damper.¹⁰

We develop the equations of motion to allow external forces and torques, but in

this paper we focus on the rotational motion free of any external forces and torques. If initially at rest the system mass center remains fixed in inertial space, although point \mathcal{O} does move with respect to inertial space as \mathcal{P} is deflected from its rest position. The model could also be used to study equilibria of orbiting dual-spin satellites by including the gravity gradient torque.

The equations of motion are developed by Hughes¹¹ in dimensional form using a Newton-Euler approach. However, we choose to non-dimensionalize the equations using a characteristic length, mass, and time. To clarify the notation, a * superscript denotes the dimensional form of each parameter or variable whereas the * is omitted once each is non-dimensionalized. The characteristic quantities selected are: length = $\sqrt{\text{tr}I^*/m^*}$, mass = m^* , and time = $\text{tr}I^*/h^*$.

These definitions produce dimensionless equations with two notable features: the trace of the dimensionless inertia matrix is always one, $\text{tr}I = 1$, and the dimensionless angular momentum vector has unit length, $\mathbf{h}^T\mathbf{h} = 1$. This latter feature is only true if $\mathbf{f} = \mathbf{g} = \mathbf{0}$.

The rotor angular momentum component along the rotor axis, $\hat{\mathbf{n}}$, of symmetry *relative to the platform*, is $\mathbf{h}_s = I_s\omega_s\hat{\mathbf{n}} = h_s\hat{\mathbf{n}}$. The *absolute* axial rotor angular momentum about $\hat{\mathbf{n}}$ is $h_a = I_s\hat{\mathbf{n}}^T\boldsymbol{\omega} + h_s = I_s(\hat{\mathbf{n}}^T\boldsymbol{\omega} + \omega_s)$. Note that h_a includes the relative angular momentum, h_s as well as a contribution from the body-frame angular velocity, $\boldsymbol{\omega}$. An important complicating feature of this system is that the system inertia matrix, J depends on x .

In dimensionless form, the equations of motion are:

$$\dot{\mathbf{p}} = -\boldsymbol{\omega}^\times \mathbf{p} + \mathbf{f} \tag{1}$$

$$\dot{\mathbf{h}} = -\boldsymbol{\omega}^\times \mathbf{h} - \mathbf{v}_o^\times \mathbf{p} + \mathbf{g} \quad (2)$$

$$\dot{h}_a = g_a \quad (3)$$

$$\dot{p}_n = \varepsilon \boldsymbol{\omega}^T \hat{\mathbf{n}}^\times [\mathbf{v}_o - (\mathbf{b} + x\hat{\mathbf{n}})^\times \boldsymbol{\omega}] - cy - kx \quad (4)$$

$$\dot{x} = y \quad (5)$$

The superscript \times denotes the skew-symmetric matrix form of a vector.¹¹ The system momenta may be expressed in terms of the system velocities as:

$$\mathbf{p} = \mathbf{v}_o - \varepsilon x \hat{\mathbf{n}}^\times \boldsymbol{\omega} + \varepsilon y \hat{\mathbf{n}} \quad (6)$$

$$\mathbf{h} = J\boldsymbol{\omega} + \varepsilon x \hat{\mathbf{n}}^\times \mathbf{v}_o + \varepsilon y \mathbf{b}^\times \hat{\mathbf{n}} + I_s \omega_s \hat{\mathbf{a}} \quad (7)$$

$$h_a = I_s (\hat{\mathbf{a}}^T \boldsymbol{\omega} + \omega_s) \quad (8)$$

$$p_n = \varepsilon (\hat{\mathbf{n}}^T \mathbf{v}_o - \hat{\mathbf{n}}^T \mathbf{b}^\times \boldsymbol{\omega} + y) \quad (9)$$

and the inertia matrix is

$$J = I + \varepsilon \left[(2x \mathbf{b}^T \hat{\mathbf{n}} + x^2) \mathbf{1} - x(\mathbf{b} \hat{\mathbf{n}}^T + \hat{\mathbf{n}} \mathbf{b}^T) - x^2 \hat{\mathbf{n}} \hat{\mathbf{n}}^T \right] \quad (10)$$

We reduce the order of the system equations by several simplifying assumptions consistent with the intention of studying the free motion of the damped gyrostat. Assuming that the external force is $\mathbf{f} = 0$, then we can set the linear momentum to $\mathbf{p} = 0$. Further assuming that the external torque is $\mathbf{g} = 0$, it follows that the angular momentum is constant. For most of the paper we also assume that $g_a = 0$ and treat h_a as a bifurcation parameter instead of as a dynamic variable. However, we do consider dual-spin turn dynamics later in the paper, in which we take the internal torque, g_a , to be a small constant. With these assumptions, we can write the velocity and angular velocity as:

$$\mathbf{v}_o = \varepsilon x \hat{\mathbf{n}}^\times \boldsymbol{\omega} - \varepsilon y \hat{\mathbf{n}} \quad (11)$$

$$\boldsymbol{\omega} = K^{-1} \mathbf{m} \quad (12)$$

where

$$\begin{aligned}
K &= I - I_s \hat{\mathbf{a}} \hat{\mathbf{a}}^T + \varepsilon \left[2x \mathbf{b}^T \hat{\mathbf{n}} E - x (\mathbf{b} \hat{\mathbf{n}}^T + \hat{\mathbf{n}} \mathbf{b}^T) - \varepsilon' x^2 \hat{\mathbf{n}}^\times \hat{\mathbf{n}}^\times \right] \\
\mathbf{m} &= \mathbf{h} - h_a \hat{\mathbf{a}} - \varepsilon y \mathbf{b}^\times \hat{\mathbf{n}} \\
\varepsilon y &= \frac{p_n + \varepsilon \hat{\mathbf{n}}^T \mathbf{b}^\times K^{-1} (\mathbf{h} - h_a \hat{\mathbf{a}})}{\varepsilon' + \varepsilon \hat{\mathbf{n}}^T \mathbf{b}^\times K^{-1} \mathbf{b}^\times \hat{\mathbf{n}}}
\end{aligned}$$

Here we have defined $\varepsilon' = 1 - \varepsilon$.

Eliminating the velocities from the equations of motion reduces the system to five scalar equations in \mathbf{h} , p_n , and x :

$$\dot{\mathbf{h}} = \mathbf{h}^\times K^{-1} \mathbf{m} \quad (13)$$

$$\dot{p}_n = -\varepsilon \mathbf{m}^T K^{-1} \hat{\mathbf{n}}^\times \left[(\mathbf{b} + \varepsilon' x \hat{\mathbf{n}})^\times K^{-1} \mathbf{m} \right] - cy - kx \quad (14)$$

$$\dot{x} = y \quad (15)$$

These equations are used in the numerical and analytical studies in this paper.

Realistic Dual-Spin Parameters

Previous works have used this dual-spin model to study equilibria in a general sense by considering an extensive range of parameter combinations.^{12–14} In this paper, we focus on a configuration that emulates realistic dual-spin satellite parameters. An axisymmetric gyrostat, defined as $I_2 = I_3$, is often used to model a dual-spin satellite.^{3,6,15} Since any real system is not perfectly axisymmetric, we examine the effects of slightly asymmetric dual-spin satellites as well as the axisymmetric case. Dual-spin satellite designers often tune the spring-mass-damper to match its natural frequency to the precession frequency of the satellite. A tuned damper is excited by the precession motion it is designed to attenuate, thereby damping out the precession

more quickly than untuned dampers. The damper spring stiffness is calculated from a simple tuning condition. Once the parameter set is determined, we use numerical continuation to characterize the equilibria of the dual-spin satellite examples.

Likins, Tseng, and Mingori studied the effects of damper nonlinearities in an attempt to explain in-flight precession data for TACSAT 1.¹⁶ We use their satellite inertia properties and damper information to generate the dimensionless parameters defined in Table 1.

Table 1: System parameters for example dual-spin satellite

Inertia Properties	Damper Parameters
$I_1 = 0.20$	$b = 0.33$
$I_2 = 0.40$	$\varepsilon = 0.01$
$I_3 = 0.40$	$c = 0.01$
$I_s = 0.14$	

We choose the desired, nominal spin configuration to have a despun platform, where $\boldsymbol{\omega} = 0$ and all the angular momentum is in the rotor, $h_a = 1$. Most dual-spin satellites have either a despun or slowly spinning platform. Typical dimensional rates, presented by Iorillo, are $\omega = 10^{-3}$ rpm and $\omega_s = 60$ rpm.¹⁵ Even for a slowly spinning platform, the despun condition is a good approximation of the desired nominal spin.

Damper Tuning

To increase the damping efficiency, we use the standard approach and match the damper natural frequency with the frequency of precession about the nominal spin.^{10,17}

$$\omega_b = \left[\frac{(I'_1 + \lambda I_2)(I'_1 + \lambda I_3)}{I_1'^2 I_2 I_3} \right]^{1/2} \quad (16)$$

where $\lambda = h_a - 1$ and $I'_1 = I_1 - I_s$. The spring-mass-damper natural frequency, without damping, is $\omega_n = \sqrt{k/\varepsilon}$. Matching the precession and damper frequencies results in the following tuned-damper condition:

$$k_d = \frac{\varepsilon (I'_1 + \lambda I_2) (I'_1 + \lambda I_3)}{I_1^2 I_2 I_3} \quad (17)$$

For the despun platform $\lambda = 0$, Eq. 17 reduces to

$$k_d = \frac{\varepsilon}{I_2 I_3} \quad (18)$$

Using this tuning condition, the damper is tuned for the dual-spin satellite example, yielding a spring stiffness, $k_d = 0.0625$. We use this spring stiffness value to produce equilibria for the dual-spin example.

Other parameters influence damper performance, such as damper position, b , and the viscous damping coefficient, c . We choose to use typical values from Ref. 16, but other researchers have considered methods to determine optimal values of damper parameters for related models.^{17,18} We proceed with the system parameters of Table 1, with a tuned damper ($k = k_d$), to examine equilibria for a dual-spin satellite.

Axisymmetric Dual-Spin Equilibria

Axisymmetric dual-spin satellites are common in the literature. But for any real system, slight inertia asymmetries will exist and are examined in the following section. For the parameter set in Table 1, we apply numerical continuation to Eqs. 13–15 to produce branches of equilibria for varying h_a . The damper is tuned for the $h_a = 1$, despun-platform condition. The equilibria are displayed on the momentum sphere and in five state-parameter bifurcation diagrams in Fig. 2. The momentum sphere representation is particularly useful because Eq. 13 implies that at equilibrium ω

is aligned with \mathbf{h} . For all these diagrams, solid lines represent stable equilibria and dashed lines indicate unstable equilibria. A dash-dot line is used to indicate stable and unstable branches for the same value of the state variable and bifurcation parameter. This overlapping of stable and unstable branches occurs for some branches of nominal-spin equilibria. For example, in h_3 - h_a bifurcation diagrams the $h_3 = 0$ axis includes both branches of $\hat{\mathbf{b}}_1$ -axis spins, $\mathbf{h} = (\pm 1, 0, 0)$.

The equilibria for this axisymmetric dual-spin satellite are in the $\hat{\mathbf{b}}_1$ - $\hat{\mathbf{b}}_2$ and $\hat{\mathbf{b}}_1$ - $\hat{\mathbf{b}}_3$ planes; except for the isolated equilibria where these branches intersect the $\hat{\mathbf{b}}_2$ - $\hat{\mathbf{b}}_3$ plane, there are no equilibria in the $\hat{\mathbf{b}}_2$ - $\hat{\mathbf{b}}_3$ plane. There are two separate bifurcation points in the h_1 - h_a bifurcation diagram (Fig. 2(b)); branches of $\hat{\mathbf{b}}_1$ -axis spins bifurcate into branches of steady spins within the $\hat{\mathbf{b}}_1$ - $\hat{\mathbf{b}}_2$ and $\hat{\mathbf{b}}_1$ - $\hat{\mathbf{b}}_3$ planes. These two bifurcation points occur for nearly the same h_a value, and they are almost indistinguishable in Fig. 2(b). Within the $\hat{\mathbf{b}}_1$ - $\hat{\mathbf{b}}_3$ plane the equilibria are stable, whereas the equilibria in the $\hat{\mathbf{b}}_1$ - $\hat{\mathbf{b}}_2$ plane are unstable. For this example, these equilibria are continuous branches without any turning points between bifurcation points (see Figs. 2(c)-2(d)). The stability of the simple $\hat{\mathbf{b}}_2$ and $\hat{\mathbf{b}}_3$ -axis spins is uncertain. For both cases, a linear stability analysis is inconclusive due to multiple zero eigenvalues. No suitable Liapunov function has been identified to provide additional stability information. However, numerical simulation of system dynamics with initial conditions near the $\hat{\mathbf{b}}_2$ and $\hat{\mathbf{b}}_3$ -axis spins indicate instability for these degenerate cases.

Analysis of the equations of motion indicates two possible $\hat{\mathbf{b}}_2$ -axis spins with zero or non-zero damper deflections. For a $\hat{\mathbf{b}}_2$ -axis spin the angular momentum vector is $\mathbf{h} = (0, \pm 1, 0)$ and $h_a = 0$. We choose to examine the $h_2 = 1$ case. The natural symmetry of the axial gyrostat with aligned damper produces symmetry in the equilibrium solutions of Eqs. 13-15. As shown in Ref. 12, the equations are invariant for

several transformations including

$$(h_1, h_2, h_3, p_n, x, h_a) \mapsto (-h_1, -h_2, h_3, -p_n, -x, -h_a) \quad (19)$$

and

$$(h_1, h_2, h_3, p_n, x, h_a) \mapsto (h_1, -h_2, -h_3, -p_n, -x, h_a) \quad (20)$$

Therefore, the equilibria for the $h_2 = -1$ spin differ from the $h_2 = 1$ case only by the opposite sign of state variables p_n and x .

For the conditions $\mathbf{h} = (0, 1, 0)$, and $h_a = 0$, the equations of motion reduce to

$$\dot{p}_n = -kx + \frac{\varepsilon\varepsilon'x(\varepsilon' - bp_n)^2}{[b^2\varepsilon - \varepsilon'(I_2 + \varepsilon\varepsilon'x^2)]^2} + \frac{c[-b\varepsilon + p_n(I_2 + \varepsilon\varepsilon'x^2)]}{\varepsilon[b^2\varepsilon - \varepsilon'(I_2 + \varepsilon\varepsilon'x^2)]} \quad (21)$$

$$\dot{x} = \frac{-b\varepsilon + p_n(I_2 + \varepsilon\varepsilon'x^2)}{\varepsilon[b^2\varepsilon - \varepsilon'(I_2 + \varepsilon\varepsilon'x^2)]} \quad (22)$$

Setting these two equations to zero, we solve for equilibrium values of p_n and x . Two possible types of equilibria exist for a $\hat{\mathbf{b}}_2$ -axis spin. The first equilibrium state is

$$(p_n, x)_1 = (b\varepsilon/I_2, 0)$$

and the second, a pair of points, is

$$(p_n, x)_{2,3} = \left(b\sqrt{\frac{\varepsilon k}{\varepsilon'}}, \pm\sqrt{\frac{\sqrt{\varepsilon\varepsilon'k} - I_2 k}{\varepsilon\varepsilon'k}} \right) \quad (23)$$

Examining Eq. 23, we see that

$$k < \varepsilon\varepsilon'/I_2^2 \quad (24)$$

defines an existence condition for the $\hat{\mathbf{b}}_2$ -axis spin with $x \neq 0$.

Equilibria not within the $\hat{\mathbf{b}}_1$ - $\hat{\mathbf{b}}_2$ or $\hat{\mathbf{b}}_1$ - $\hat{\mathbf{b}}_3$ planes do not exist for this axisymmetric case. However, these type of equilibria are possible for larger values of spring stiffness. Reference 12 identified such branches of equilibria which always include the $\hat{\mathbf{b}}_2$ -axis

spin with $x \neq 0$. These equilibrium branches originate from bifurcation points in the $\hat{\mathbf{b}}_1$ – $\hat{\mathbf{b}}_2$ or $\hat{\mathbf{b}}_1$ – $\hat{\mathbf{b}}_3$ planes. Although not rigorous, numerical continuation results suggest that the existence of these out-of-plane equilibria corresponds to the existence of $\hat{\mathbf{b}}_2$ -axis spins with $x \neq 0$. We look more closely at the example axisymmetric gyrostat for k values near the $\hat{\mathbf{b}}_2$ -axis spin ($x \neq 0$) existence threshold, defined by Eq. 24. Figure 3 shows the equilibria for k just lower and higher than the existence threshold.

For $k = 0.06187 < \varepsilon\varepsilon'/I_2^2$, the equilibria include the $\hat{\mathbf{b}}_2$ -axis spin and equilibrium branches in the $\hat{\mathbf{b}}_2$ – $\hat{\mathbf{b}}_3$ plane, whereas these equilibria do not occur for $k = 0.06188 > \varepsilon\varepsilon'/I_2^2$.

The existence threshold of Eq. 24 is related to the damper tuning condition of k . We examine this relationship by noting that the existence condition is similar to the tuned-damper condition for a despun platform, Eq. 18. Expanding Eq. 24 in terms of ε , we relate the existence condition to the tuned-damper value, k_d , assuming an axisymmetric gyrostat ($I_2 = I_3$):

$$k < \varepsilon/I_2^2 - \varepsilon^2/I_2^2 = k_d(1 - \varepsilon) = \varepsilon'k_d \quad (25)$$

Therefore, the classic damper tuning condition produces a k_d value greater than the existence threshold for the $\hat{\mathbf{b}}_2$ -axis spin with $x \neq 0$. This equilibrium state does not exist for $k = k_d$. For small ε , k_d is also near the existence threshold for nearly axisymmetric gyrostats ($I_2 \approx I_3$). Because of this result, we find that out-of-plane equilibria are not prevalent for nearly axisymmetric dual-spin satellites with tuned dampers.

Nearly Axisymmetric Dual-Spin Equilibria

We consider the effects of a slightly asymmetric platform on the equilibria for the example dual-spin satellite. We examine two cases: $I_2 > I_3$ and $I_3 > I_2$. The parameter set remains unchanged except for these two inertia values. The tuned-damper value of k does not change appreciably for these inertia properties. In the first example, we use $\mathbf{I} = (0.20, 0.41, 0.39)$ and in the second example, $\mathbf{I} = (0.20, 0.39, 0.41)$. We apply numerical continuation to the prolate dual-spin satellite, with $I_2 > I_3$, to produce equilibria for varying h_a , shown as Fig. 4. For the $I_3 > I_2$ example, the results are shown as Fig. 5.

We see in Fig. 4 that for $I_2 > I_3$ the stability of $\hat{\mathbf{b}}_1\text{--}\hat{\mathbf{b}}_3$ and $\hat{\mathbf{b}}_1\text{--}\hat{\mathbf{b}}_2$ plane equilibria differs from the axisymmetric case. The $\hat{\mathbf{b}}_1\text{--}\hat{\mathbf{b}}_2$ plane equilibria and the $\hat{\mathbf{b}}_2$ -axis spin, with $x = 0$, are stable. The $\hat{\mathbf{b}}_1\text{--}\hat{\mathbf{b}}_3$ plane equilibria and the $\hat{\mathbf{b}}_3$ -axis spin are unstable. As with the axisymmetric case, the $\hat{\mathbf{b}}_2$ -axis spin with $x \neq 0$ does not exist. The slight increase in I_2 , relative to the axisymmetric example, lowers the existence threshold to $k < 0.059$ and is lower than the tuned-damper value of $k = 0.0625$.

Figure 5 shows that for $I_3 > I_2$, $\hat{\mathbf{b}}_1\text{--}\hat{\mathbf{b}}_3$ plane equilibria are stable, whereas $\hat{\mathbf{b}}_1\text{--}\hat{\mathbf{b}}_2$ plane equilibria are unstable. The slight decrease in I_2 , relative to the axisymmetric example, raises the existence threshold to $k < 0.065$. For the tuned-damper value, $k = 0.0625$, a $\hat{\mathbf{b}}_2$ -axis spin with $x \neq 0$ is a possible equilibrium state. This configuration also has relatively small out-of-plane equilibrium branches near the $\hat{\mathbf{b}}_2$ -axis spin, best seen in Fig. 5(d), although these off-axis equilibria are unstable.

Reference 12 demonstrates that decreasing k affects the out-of-plane equilibrium branches. For lower k values, the branches have larger h_3 components. For sufficiently small k , the out-of-plane equilibria intersect branches of equilibria in the $\hat{\mathbf{b}}_1\text{--}\hat{\mathbf{b}}_3$ plane at bifurcation points. For prolate gyrostats with $I_2 > I_3$, the out-of-plane equilibria

can be stable and are potential trap states for systems disturbed from their nominal spin. These stable, out-of-plane branches can affect the dynamics of maneuvers that use rotor torques to change the system attitude. In the next section we consider a simple maneuver using small rotor torques, and how stable out-of-plane branches of equilibria affect the motion.

Spinup Dynamics

In this section we examine how different system parameter sets affect the path of \mathbf{h} in state space during a rotor spinup maneuver called a dual-spin turn.⁹ A dual-spin turn may be used to deploy a dual-spin satellite from an initial configuration, with locked damper and rotor, to its final, despun platform, configuration. Because the typical dual-spin satellite is prolate, its initial configuration is a major-axis spin. The dual-spin turn involves applying a small rotor torque until the rotor is in its final, $h_a = 1$, state. The satellite spin-axis transitions from the major-axis to the nominal (minor), $\hat{\mathbf{b}}_1$ -axis. The bifurcation diagrams for varying h_a provide a useful perspective on the dynamics of the dual-spin turn. For spinup maneuvers with sufficiently small g_a , the system state approximately follows branches of stable equilibria for increasing h_a . We simulate the dual-spin turn dynamics for the two nearly-axisymmetric dual-spin satellites of the previous section by numerically integrating Eqs. 1–5. Depending on the parameter set, the path of the \mathbf{h} vector in state-space may vary significantly.

The steps in the dual-spin turn are: 1) unlock the damper and let the system reach equilibrium; 2) apply a small, constant g_a until $h_a = 1$; and 3) allow the damper to dissipate any residual coning motion. We first consider the asymmetric dual-spin satellite with $I_3 > I_2$, shown in Fig 6, with a tuned damper. Because the equilibrium

branches are relatively simple for this configuration, \mathbf{h} transitions along the $\hat{\mathbf{b}}_1$ – $\hat{\mathbf{b}}_3$ plane for a dual-spin turn from the $\hat{\mathbf{b}}_3$ -axis spin to the $\hat{\mathbf{b}}_1$ -axis spin, approximately following the stable branch of equilibria in the $\hat{\mathbf{b}}_1$ – $\hat{\mathbf{b}}_3$ plane. Figure 6(a) shows the path of \mathbf{h} on the momentum sphere and Fig. 6(b) the damper displacement time history.

We use $g_a = 0.001$, requiring 1000 dimensionless time units (TU) to spinup the rotor. The stable $\hat{\mathbf{b}}_3$ -axis spin has $x = 0$, so the 100 TU allowed for the damper to stabilize is much longer than required. As $h_a \rightarrow 1$, the system experiences a coning motion around the nominal spin axis. After the rotor torque ends, and $h_a = 1$, the damper dissipates the precession as the system approaches the nominal spin asymptotically.

We simulate the dynamics of a dual-spin turn for the $I_2 > I_3$ configuration of Fig. 4. The system transitions from a $\hat{\mathbf{b}}_2$ -axis spin to a $\hat{\mathbf{b}}_1$ -axis spin, approximately following the stable equilibrium branch in the $\hat{\mathbf{b}}_1$ – $\hat{\mathbf{b}}_2$ plane. Figure 7 illustrates the dual-spin dynamics on the momentum sphere and the damper displacement history. The results are similar to the $I_3 > I_2$ configuration: the \mathbf{h} vector transitions in a direct fashion to near the nominal spin, precesses slightly, and is damped to the desired nominal spin state. All equilibria in the $\hat{\mathbf{b}}_1$ – $\hat{\mathbf{b}}_2$ plane have $x = 0$ so the damper remains largely undisplaced until the precession begins.

In the previous two examples, the equilibria did not include stable off-axis equilibria, due to the tuned-damper value of k . As discussed in Ref. 12, decreasing k results in more pronounced and potentially complex out-of-plane equilibria. For systems with $k < k_d$, the dual-spin turn dynamics are not as simple as for systems with tuned dampers.

We repeat the simulation of the $I_2 > I_3$ configuration, but for $k = 0.04$. Figure 8 shows the dynamics on the momentum sphere and the damper displacement history. As with earlier simulations, the rotor torque is small: $g_a = 0.001$. The lower value of k changes the stability properties of the major-axis spin: a $\hat{\mathbf{b}}_2$ -axis spin with $x \neq 0$ is stable whereas the spin with $x = 0$ is unstable. The unlocked damper stabilizes at a non-zero value of x . This large damper displacement may not be physically feasible for real damper designs, but we do not restrict x in the simulation. The system oscillates slightly as \mathbf{h} first follows the stable out-of-plane equilibria then the branches of equilibria in the $\hat{\mathbf{b}}_1$ - $\hat{\mathbf{b}}_2$ plane. As with previous examples, the system experiences coning motion as \mathbf{h} approaches $\hat{\mathbf{b}}_1$. This example illustrates how the transition of the spin axis from major to minor axis may not necessarily follow a simple path. However, the branches of stable equilibria for increasing h_a predict the spin-axis path for the dual-spin turn.

Reference 12 shows that for sufficiently small k , the out-of-plane equilibria intersect the $\hat{\mathbf{b}}_1$ - $\hat{\mathbf{b}}_3$ plane equilibria at bifurcation points. For these low values of k , the spinup dynamics are significantly affected. We examine the same $I_2 > I_3$ configuration, but for $k = 0.005$. Figure 9 shows the spinup dynamics displayed on the momentum sphere for this configuration using two different rotor torques. In Fig. 9(a), we use $g_a = 0.001$. For this rotor torque, \mathbf{h} transitions in the direction of the stable out-of-plane branch, then the stable branch in the $\hat{\mathbf{b}}_1$ - $\hat{\mathbf{b}}_3$ plane. The system oscillates more than examples with larger k , and \mathbf{h} only roughly follows the out-of-plane equilibria. The abrupt change at the bifurcation point produces more oscillation, but \mathbf{h} proceeds roughly along the $\hat{\mathbf{b}}_1$ - $\hat{\mathbf{b}}_3$ branch toward the nominal spin. However, this branch is not entirely stable; there is a bifurcation point, with out-of-plane equilibria forming a ring around the $\hat{\mathbf{b}}_1$ axis. The stability change at the bifurcation point

produces a jump phenomenon, and \mathbf{h} jumps toward stable equilibria in the $\hat{\mathbf{b}}_1$ – $\hat{\mathbf{b}}_2$ plane before beginning precession followed by damping to the nominal spin. Smaller rotor torques allow \mathbf{h} to more closely follow the stable branches, but also lengthen the spinup time. In Fig. 9(b) we use $g_a = 0.0001$, which reduces the system oscillation and allows \mathbf{h} to more closely follow stable branches of equilibria. However, the spinup maneuver requires 10,000 TU.

Conclusions

Equilibria of dual-spin satellites are affected by varying system parameters, but for typical parameter values the set of equilibria is relatively simple. Whereas a perfectly axisymmetric gyrostat has fewer branches of equilibria than asymmetric configurations, slight inertia asymmetries produce additional possible equilibria. For tuned dampers, the spring stiffness is sufficiently large to produce continuous branches of equilibria that primarily lie in principal planes. The bifurcation results for varying rotor momentum provide a unique perspective on the dynamics of rotor spinup. For a tuned damper, the dual-spin turn transitions directly along principal planes toward the nominal spin equilibrium. The spinup dynamics are more complex if the spring stiffness is less than the tuned-damper value, possibly resulting in jump phenomena.

Acknowledgements

The first author has been supported by the Air Force Institute of Technology’s Civilian Institutions program for Air Force Academy Faculty Preparation. The second author has been supported by the Air Force Office of Scientific Research and the National Science Foundation.

Disclaimer

The views expressed in this article are those of the authors and do not reflect the official policy or position of the United States Air Force, Department of Defense, or the US Government.

References

- [1] Likins, P. W., “Spacecraft Attitude Dynamics and Control — A Personal Perspective on Early Developments,” *Journal of Guidance, Control, and Dynamics*, Vol. 9, No. 2, 1986, pp. 129–134.
- [2] Landon, V. D. and Stewart, B., “Nutational Stability of an Axisymmetric Body Containing a Rotor,” *Journal of Spacecraft and Rockets*, Vol. 1, No. 6, 1964, pp. 682–684.
- [3] Likins, P. W., “Attitude Stability Criteria for Dual Spin Spacecraft,” *Journal of Spacecraft and Rockets*, Vol. 4, No. 12, 1967, pp. 1638–1643.
- [4] Hall, C. D., “Spinup Dynamics of Gyrostats,” *Journal of Guidance, Control, and Dynamics*, Vol. 18, No. 5, 1995, pp. 1177–1183.
- [5] Cloutier, G. J., “Nutation Damper Instability on Spin-Stabilized Spacecraft,” *AIAA Journal*, Vol. 7, No. 11, 1969, pp. 2110–2115.
- [6] Mingori, D. L., “Effects of Energy Dissipation on the Attitude Stability of Dual-Spin Satellites,” *AIAA Journal*, Vol. 7, No. 1, 1969, pp. 20–27.

- [7] Cochran, J. E. and Shu, P. H., “Effects of Energy Addition and Dissipation on Dual-Spin Spacecraft Attitude Motion,” *Journal of Guidance, Control, and Dynamics*, Vol. 6, No. 5, 1983, pp. 368–373.
- [8] Seydel, R., *Practical Bifurcation and Stability Analysis*, Springer-Verlag, New York, 2nd edition, 1994.
- [9] Hubert, C. H., “Dynamics of the Generalized Dual-Spin Turn,” *RCA Review*, Vol. 41, No. 3, 1980, pp. 449–471.
- [10] Schneider, C. C. and Likins, P. W., “Nutation Dampers vs Precession Dampers for Asymmetric Spinning Spacecraft,” *Journal of Spacecraft and Rockets*, Vol. 10, No. 3, 1973, pp. 218–222.
- [11] Hughes, P. C., *Spacecraft Attitude Dynamics*, John Wiley and Sons, New York, 1986, pp. 217–221.
- [12] Sandfry, R. A., *Equilibria of a Gyrostat with a Discrete Damper*, PhD thesis, Virginia Polytechnic Institute and State University, July 2001.
- [13] Sandfry, R. A. and Hall, C. D., “Motion of a Gyrostat with a Discrete Damper,” AIAA 00-4534, Aug 2000.
- [14] Sandfry, R. A. and Hall, C. D., “Relative Equilibria of a Gyrostat with a Discrete Damper,” *Proceedings of the AAS/AIAA Astrodynamics Specialist Conference*, Quebec City, Canada, Aug 2001, pp. 1683–1702.
- [15] Iorillo, A. J., “Hughes Gyrostat System,” *Proceedings of the Symposium on Attitude Stabilization and Control of Dual-Spin Spacecraft*, Editors William J. Russell and Curtiss R. Lee, El Segundo, CA, 1967. Air Force Systems Command and Aerospace Corporation, pp. 256–266,.

- [16] Likins, P. W., Tseng, G.-T., and Mingori, D. L., “Stable Limit Cycles due to Nonlinear Damping in Dual-Spin Spacecraft,” *Journal of Spacecraft and Rockets*, Vol. 8, No. 6, 1971, pp. 568–574.
- [17] Sarychev, V. A. and Sazonov, V. V., “Spin-Stabilized Satellites,” *Journal of the Astronautical Sciences*, Vol. 24, No. 4, 1976, pp. 291–310.
- [18] Amieux, J. C. and Dureigne, M., “Analytical Design of Optimal Nutation Dampers,” *Journal of Spacecraft and Rockets*, Vol. 9, No. 12, 1972, pp. 934–935.

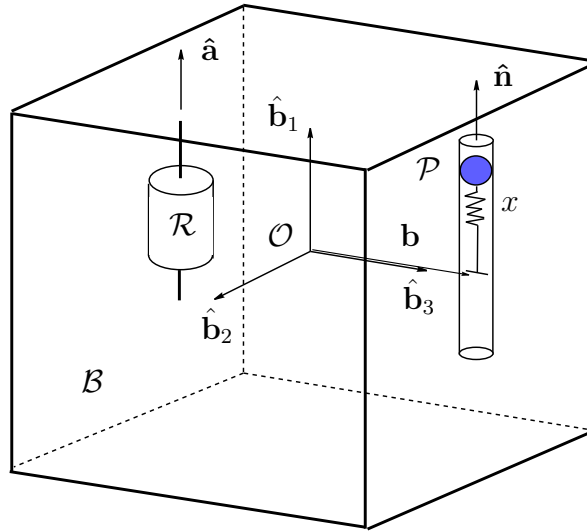
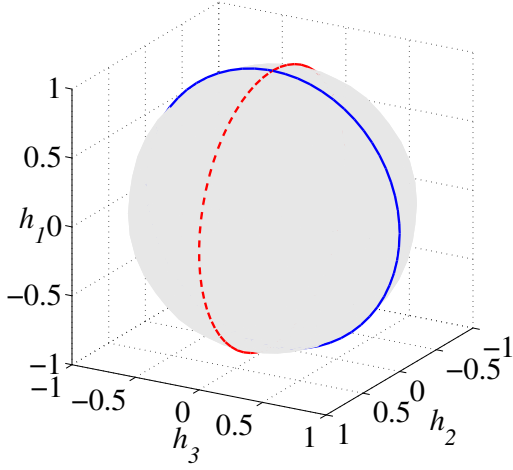
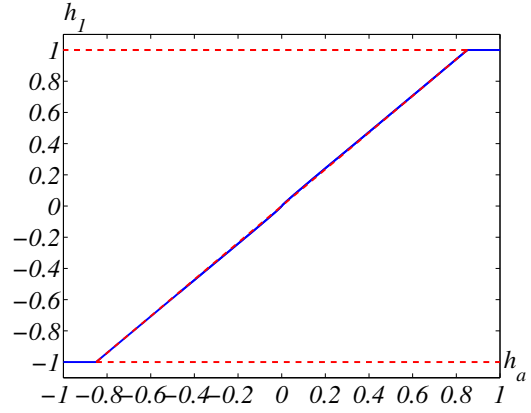


Figure 1: Single-rotor axial gyrostatt with aligned discrete damper

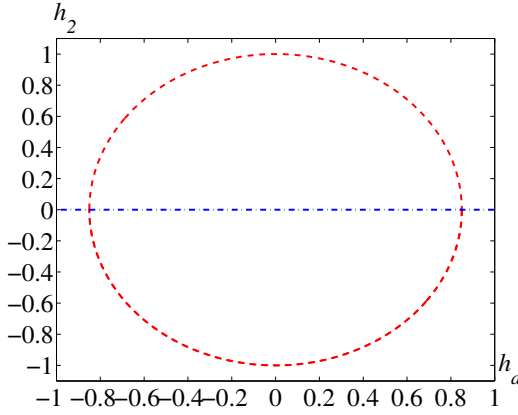
Sandfry
& Hall
Fig. 1



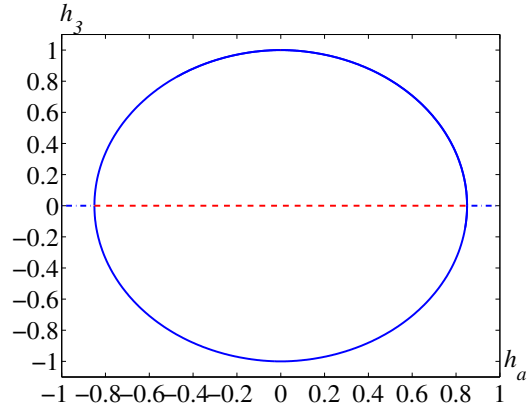
(a) Momentum sphere



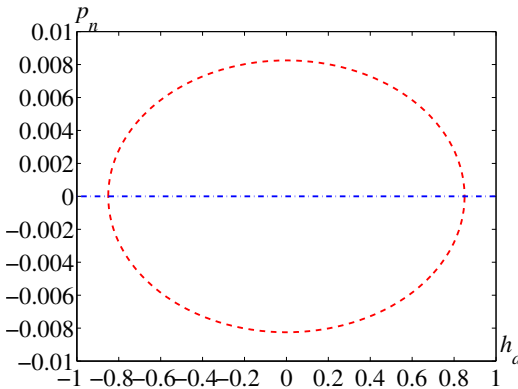
(b) h_1 vs. h_a



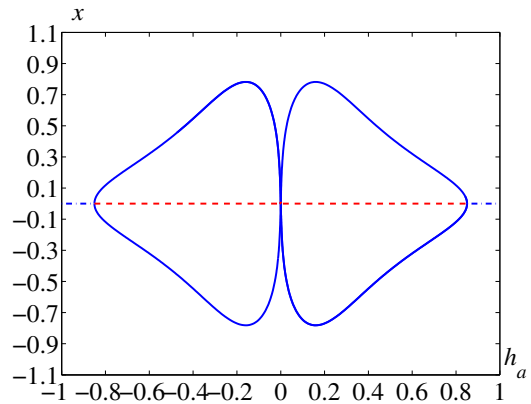
(c) h_2 vs. h_a



(d) h_3 vs. h_a



(e) p_n vs. h_a



(f) x vs. h_a

Figure 2: Bifurcation diagrams for axisymmetric dual-spin satellite

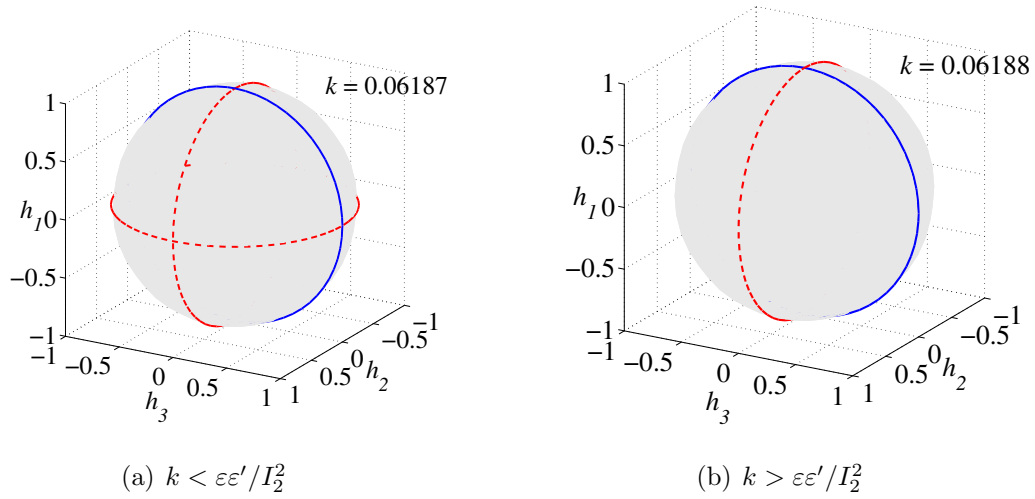


Figure 3: Axisymmetric dual-spin satellite equilibria near Type 2B existence threshold, $k = \varepsilon\varepsilon'/I_2^2 = 0.061875$

Sandfry
& Hall
Fig. 3

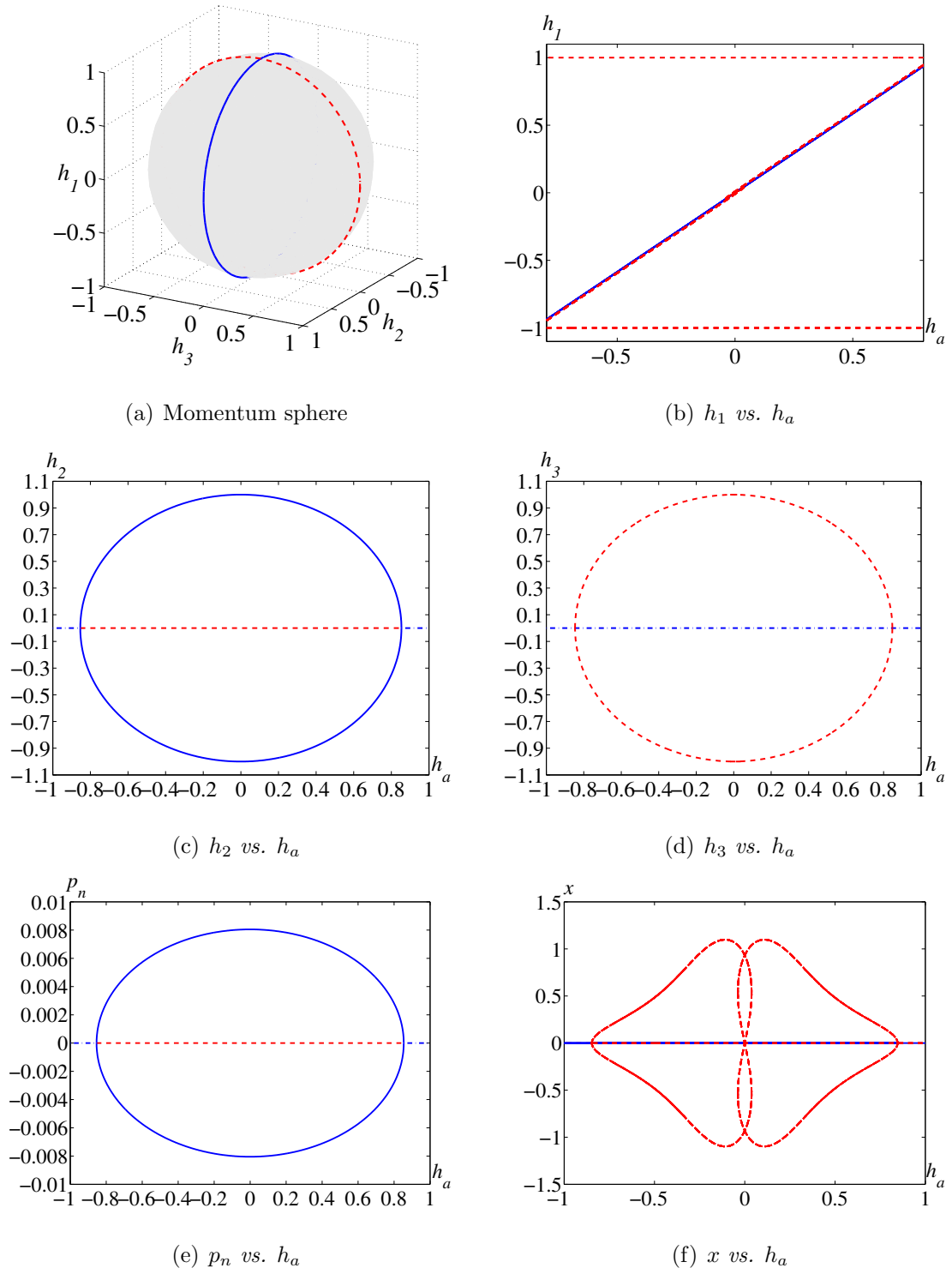
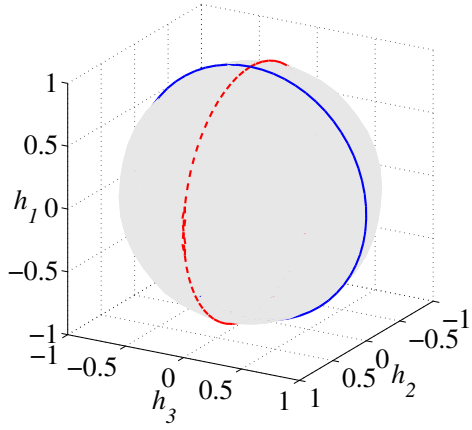
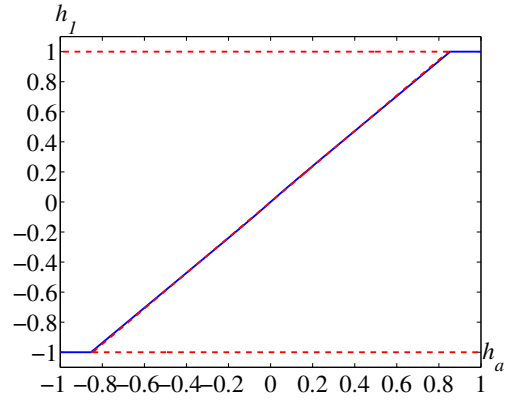


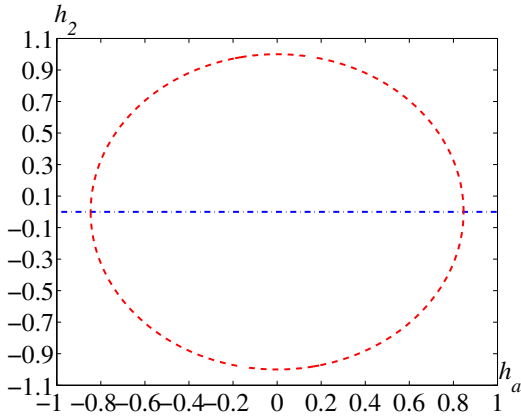
Figure 4: Bifurcation diagrams for near-axisymmetric dual-spin satellite, $I_2 > I_3$



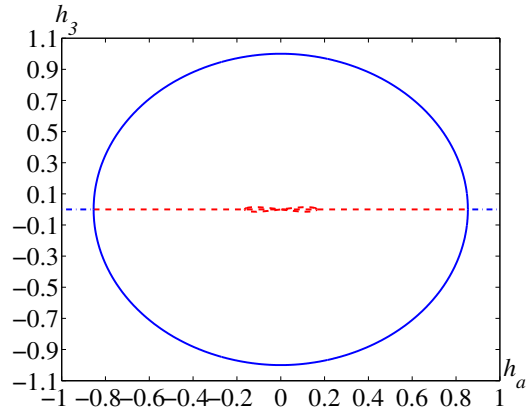
(a) Momentum sphere



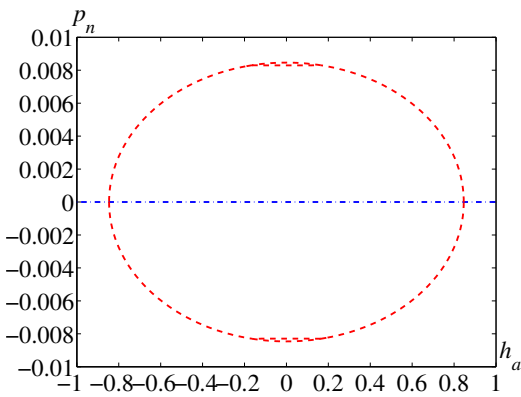
(b) h_1 vs. h_a



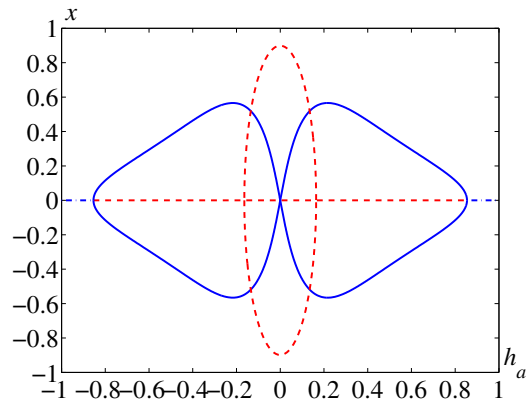
(c) h_2 vs. h_a



(d) h_3 vs. h_a

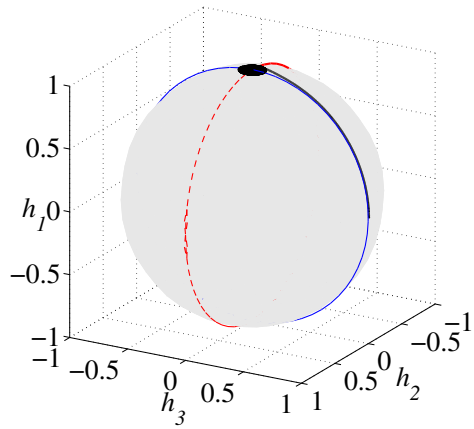


(e) p_n vs. h_a

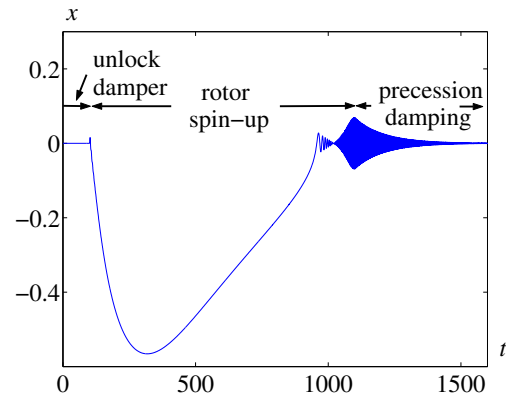


(f) x vs. h_a

Figure 5: Bifurcation diagrams for near-axisymmetric dual-spin satellite, $I_3 > I_2$



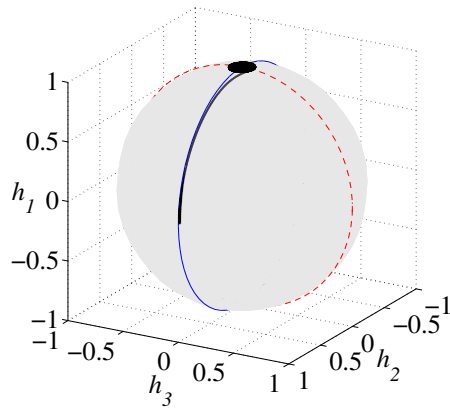
(a) Path of \mathbf{h} on the momentum sphere



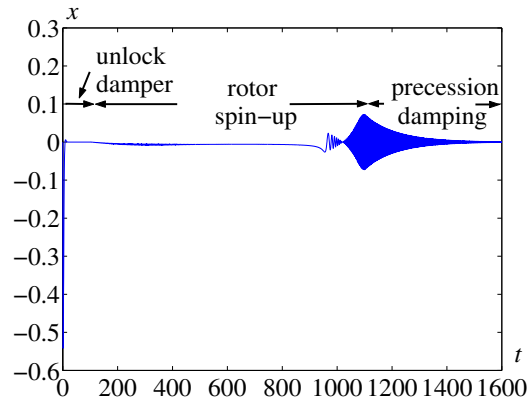
(b) Damper displacement during dual-spin turn

Figure 6: Dynamics of dual-spin turn for near-axisymmetric, prolate dual-spin satellite, $I_3 > I_2$

Sandfry
& Hall
Fig. 6



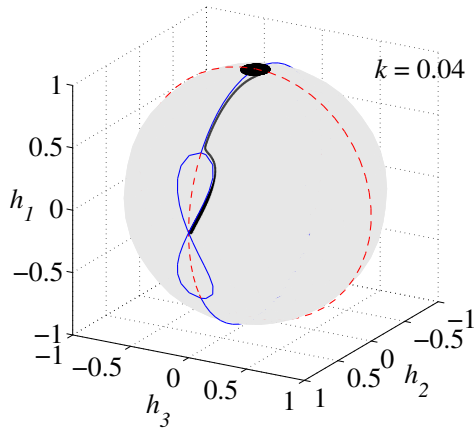
(a) Path of \mathbf{h} on the momentum sphere



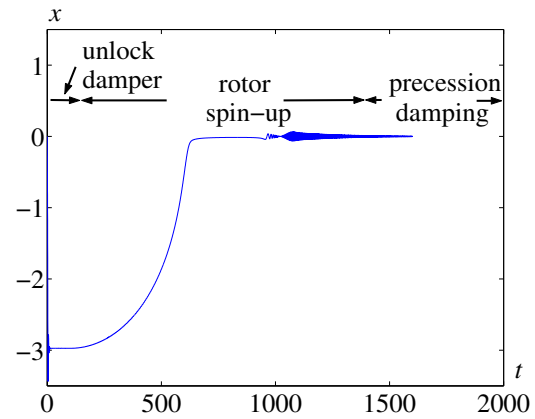
(b) Damper displacement during dual-spin turn

Figure 7: Dynamics of dual-spin turn for near-axisymmetric, prolate dual-spin satellite, $I_2 > I_3$

Sandfry
& Hall
Fig. 7



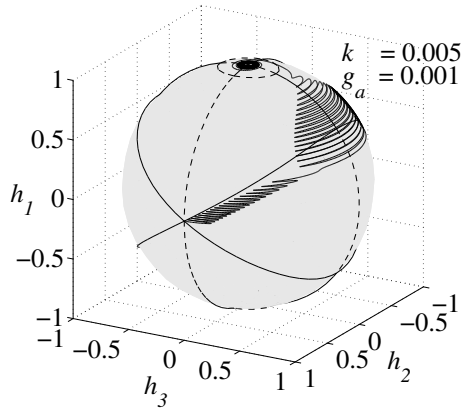
(a) Path of \mathbf{h} on the momentum sphere



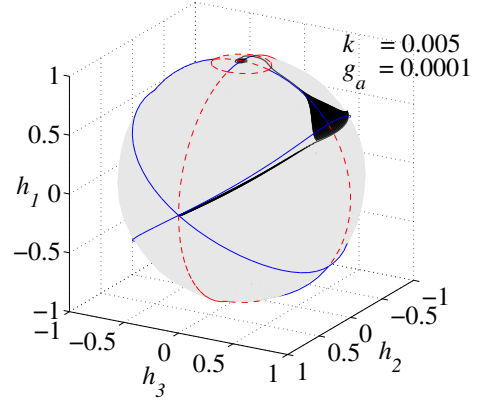
(b) Damper displacement during dual-spin turn

Figure 8: Dynamics of dual-spin turn for prolate dual-spin satellite ($I_2 > I_3$) with $k < k_d$

Sandfry
& Hall
Fig. 8



(a) Path of \mathbf{h} on the momentum sphere,
 $g_a = 0.001$



(b) Path of \mathbf{h} on the momentum sphere,
 $g_a = 0.0001$

Figure 9: Dynamics of dual-spin turn for prolate dual-spin satellite ($I_2 > I_3$) with $k \ll k_d$

Sandfry
 & Hall
 Fig. 9